Supplement of Biogeosciences, 23, 8457–8475, 2026
https://doi.org/10.5194/bg-23-8457-2026-supplement
© Author(s) 2026. CC BY 4.0 License.



Biogeosciences Open Access EGU

Supplement of

Acidification in coastal waters of Adélie Land, Antarctica (1985–2025)

Nicolas Metzl et al.

Correspondence to: Nicolas Metzl (nicolas.metzl@locean.ipsl.fr)

The copyright of individual parts of the supplement might differ from the article licence.

This document includes Table S1-S3 and Figures S1-S15 providing the supplementary information 16 that supports part of the discussion presented in the main article.

Table S1: List of cruises in the region south of 60°S from SOCAT-v2025 (Bakker et al, 2025) and new data in 2025.

EXPOCODE	Year	Month	Ship	Principal Investigator	Flag
49HH19831123	1984	1	Hakuho Maru	Inoue, H.	D
09AR19910926	1991	10	Aurora Australis	Tilbrook, B.	B
09AR19930311	1993	3	Aurora Australis	Tilbrook, B.	C
09AR19940101	1994	1	Aurora Australis	Tilbrook, B.	B
49HH19941123	1994	12	Hakuho Maru	Inoue, H.	D
09AR19941213	1995	1	Aurora Australis	Tilbrook, B.	B
320619950317	1995	3	Nath. B. Palmer	Takahashi, T. : Sweeney, C. : Sutherland, S.C.	D
09AR19950717	1995	7	Aurora Australis	Tilbrook, B.	B
09AR19950916	1995	9	Aurora Australis	Tilbrook, B.	C
09AR19960119	1996	3	Aurora Australis	Tilbrook, B.	C
09AR19960822	1996	8	Aurora Australis	Tilbrook, B.	C
353L19961021	1996	10	L_Astrolabe	Metzl, N.	D
353L19970202	1997	2	L_Astrolabe	Metzl, N.	D
09AR19980715	1998		Aurora Australis	Tilbrook, B.	B
61TG19990202	1999	2	Tangaroa	Bakker, D.	D
09AR19990716	1999	8	Aurora Australis	Tilbrook, B.	B
320620001220	2000	12	Nath. B. Palmer	Takahashi, T. : Sweeney, C. : Sutherland, S.C.	D
320620010130	2001	2	Nath. B. Palmer	Takahashi, T. : Sweeney, C. : Sutherland, S.C.	B
09AR20011031	2001	10	Aurora Australis	Tilbrook, B.	B
49HH20011128	2002	1	Hakuho Maru	Inoue, H.	D
35MF20030126*	2003	2	Marion Dufresne	Metzl, N.	D
320620041012	2004	10	Nath. B. Palmer	Takahashi, T. : Sweeney, C. : Sutherland, S.C.	B
353L20041230*	2005	1	L_Astrolabe	Goyet, C.	D
353L20050218*	2005	2	L_Astrolabe	Goyet, C.	D
353L20051019*	2005	10	L_Astrolabe	Goyet, C.	D
33RR20070204	2007	2	Roger Revelle	Wanninkhof, R.	D
49QB20080125	2008	2	Umitaka Maru	Hashida, G.	B
353L20090101*	2009	1	L_Astrolabe	Tilbrook, B.	B
353L20090109*	2009	1	L_Astrolabe	Tilbrook, B.	B
353L20090122*	2009	1	L_Astrolabe	Tilbrook, B.	B
353L20090218*	2009	2	L_Astrolabe	Tilbrook, B.	B
353L20090227*	2009	2	L_Astrolabe	Tilbrook, B.	B
353L20091021*	2009	10	L_Astrolabe	Tilbrook, B.	B
353L20091111*	2009	11	L_Astrolabe	Tilbrook, B.	B
353L20100219*	2010	2	L_Astrolabe	Tilbrook, B.	B
353L20100228*	2010	2	L_Astrolabe	Tilbrook, B.	B
353L20101021*	2010	10	L_Astrolabe	Tilbrook, B.	B
353L20101031*	2010	11	L_Astrolabe	Tilbrook, B.	B
09AR20110104	2011	1	Aurora Australis	Tilbrook, B.	B
353L20110220*	2011	2	L_Astrolabe	Tilbrook, B.	B
353L20110301*	2011	3	L_Astrolabe	Tilbrook, B.	B
09AR20120105	2012	1	Aurora Australis	Tilbrook, B.	A
353L20120107*	2012	1	L_Astrolabe	Tilbrook, B.	A
353L20120123*	2012	1	L_Astrolabe	Tilbrook, B.	B
353L20120218*	2012	2	L_Astrolabe	Tilbrook, B.	B
353L20120302*	2012	3	L_Astrolabe	Tilbrook, B.	B
353L20121013*	2012	10	L_Astrolabe	Tilbrook, B.	B
353L20121118*	2012	11	L_Astrolabe	Tilbrook, B.	B

49NZ20121128*	2012	12	Mirai	Murata, A.	A		
353L20130110	2013	1	L_Astrolabe	Tilbrook, B.	B		
353L20130126	2013	1	L_Astrolabe	Tilbrook, B.	B		
353L20130219*	2013	2	L_Astrolabe	Tilbrook, B.	B		
61TG20130202	2013	2	Tangaroa	Currie, K.I.	C		
353L20130226*	2013	3	L_Astrolabe	Tilbrook, B.	B		
320620140129	2014	2	Nat. B. Palmer	Takahashi, T. : Sweeney, C. : Sutherland, S.C.			D
09AR20141205	2015	1	Aurora Australis	Tilbrook, B.	B		
09AR20161208	2016	12	Aurora Australis	Tilbrook, B.	A		
09AR20161208	2017	1	Aurora Australis	Tilbrook, B.	A		
096U20180111	2018	2	Investigator	Tilbrook, B.	A		
49KD20181212	2019	1	Kaiyo-maru	Nomura, D.	C		
096U20190118	2019	1	Investigator	Tilbrook, B.	B		
09AR20191201	2019	12	Aurora Australis	Tilbrook, B.	B		
WFCH20230214	2023	2	Le Cdt Charcot	Wanninkhof, R. : Pierrot, D.		B	
096U20240105	2024	1	Investigator	Tilbrook, B. : Akl, J. : Neill, C.		B	
SOCISSE R2 *	2024	12	L_Astrolabe	Tilbrook, B. : Akl, J	N		
SOCISSE R3	2025	1	L_Astrolabe	Tilbrook, B. : Akl, J	N		
SOCISSE R4	2025	2	L_Astrolabe	Tilbrook, B. : Akl, J	N		

(*) For these cruises discrete or underway A_T C_T data available at https://doi.org/10.17882/102337

Table S2: List of cruises in the Adélie Land region (south of 63°S) from GLODAPv2.2023 (Lauvset et al, 2023, 2024) used for both surface C_T and C_{ant} estimate. The column C_{ant} identify cruises with available A_T and C_T data for C_{ant} estimates. All cruises are also used for surface data. Month indicate the season for data south of 63°S used for the trend analysis.

EXPOCODE	Year	Month	Carbon P.I.	C_{ant}
09AR19930404	1993	4	B. Tilbrook	
09AR19940101	1994	1	B. Tilbrook	
49HH19941213	1994	12	M. Ishii	Yes
09AR19941213	1995	1	M. Ishii	Yes
09AR19950717	1995	7	B. Tilbrook	
09AR19960119	1996	3	B. Tilbrook	
09AR19960822	1996	8	B. Tilbrook	Yes
09AR20011029	2001	11	B. Tilbrook	Yes
49HH20011127	2002	1	M. Ishii	
61TG20020206	2002	2	M. Ishii	
OISO-10	2003	2	N. Metzl	Yes
61TG20030217	2003	3	M. Ishii	
09AR20071216	2007	12	B. Tilbrook	Yes
09AR20080322	2008	3	B. Tilbrook	Yes
09AR20110104	2011	1	B. Tilbrook	
09AR20120105	2012	1	B. Tilbrook	
49NZ20121128	2012	12	A. Murata	
09AR20141205	2015	1	B. Tilbrook	Yes
096U20180111	2018	1	B. Tilbrook	Yes

Table S3: Trend of C_T and pH over 1985-2025 at location 140°E/65.75°S deduced from the FFNN model using A_T from LIAR or A_T from Eq 1.

Period, Method	C_T µmol/kg/yr	pH /yr
January Using LIAR	+0.080	-0.000675
January Using Eq 1	+0.097	-0.000650
August Using LIAR	+0.443	-0.00131
August Using Eq 1	+0.447	-0.001315

Figure S1: Sea surface fCO_2 (µatm) observed in December 2024/January 2025 (R2), January-February 2025 (R3) and February 2025 (R4) along the track between Hobart and Adélie Land. In this study only data south of 63°S are used for the trend analysis. The red dashed line is the mean atmospheric CO_2 concentration in January 2025 at Cap Grim or at South Pole (422 ppm). (https://gml.noaa.gov/dv/iadv/).

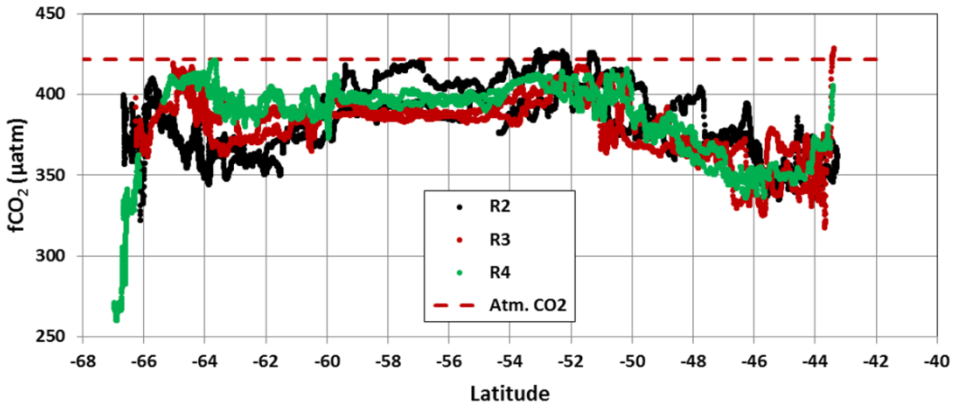


Figure S2: Sea surface A_T and C_T concentrations (µmol kg^{-1}) observed in January 2025 along the track between Hobart and Adélie Land. The red symbols indicate suspicious data. In this study only data south of 63°S are used.

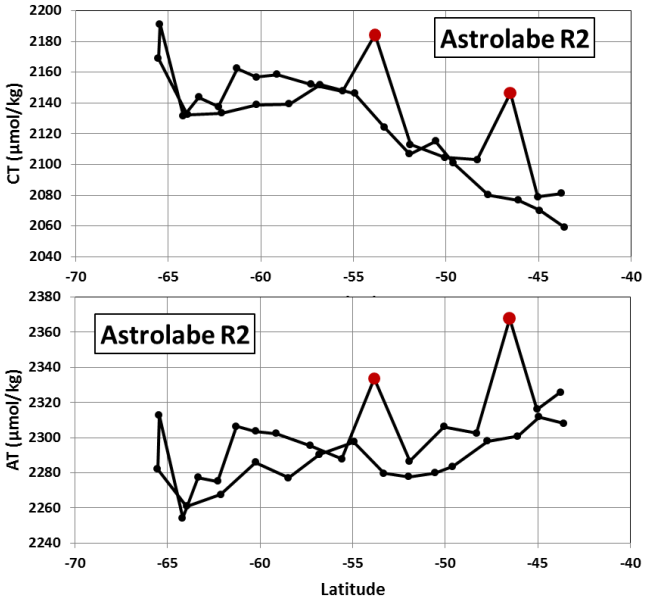


Figure S3: Sea surface silicates (black circles) and phosphates (open circles) concentrations (µmol kg^{-1}) observed in February 2003 along the track between Hobart and Adélie Land (OISO-10 cruise). At high latitudes values for silicates of 40 µmol kg^{-1} and phosphates of 2 µmol kg^{-1} were used for pH and Ω_{ar} calculations using CO2sys.

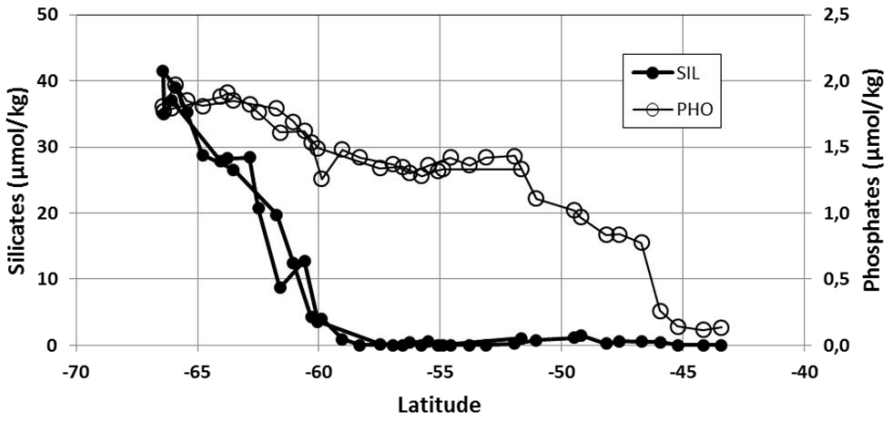


Figure S4: (a) Sea surface A_T distribution (color code in µmol kg^{-1}) in the region from GLODAP and SNAPO-CO2 data available between 1995 and 2018. (b) A_T (µmol kg^{-1}) versus salinity from these data and used to calculate the A_T/salinity relationship (red dashed). Also shown are the relationships from Stark et al (2018), Lee et al (2006) or using only GLODAP data (green). Figure (a) produced with ODV (Schlitzer, 2018).

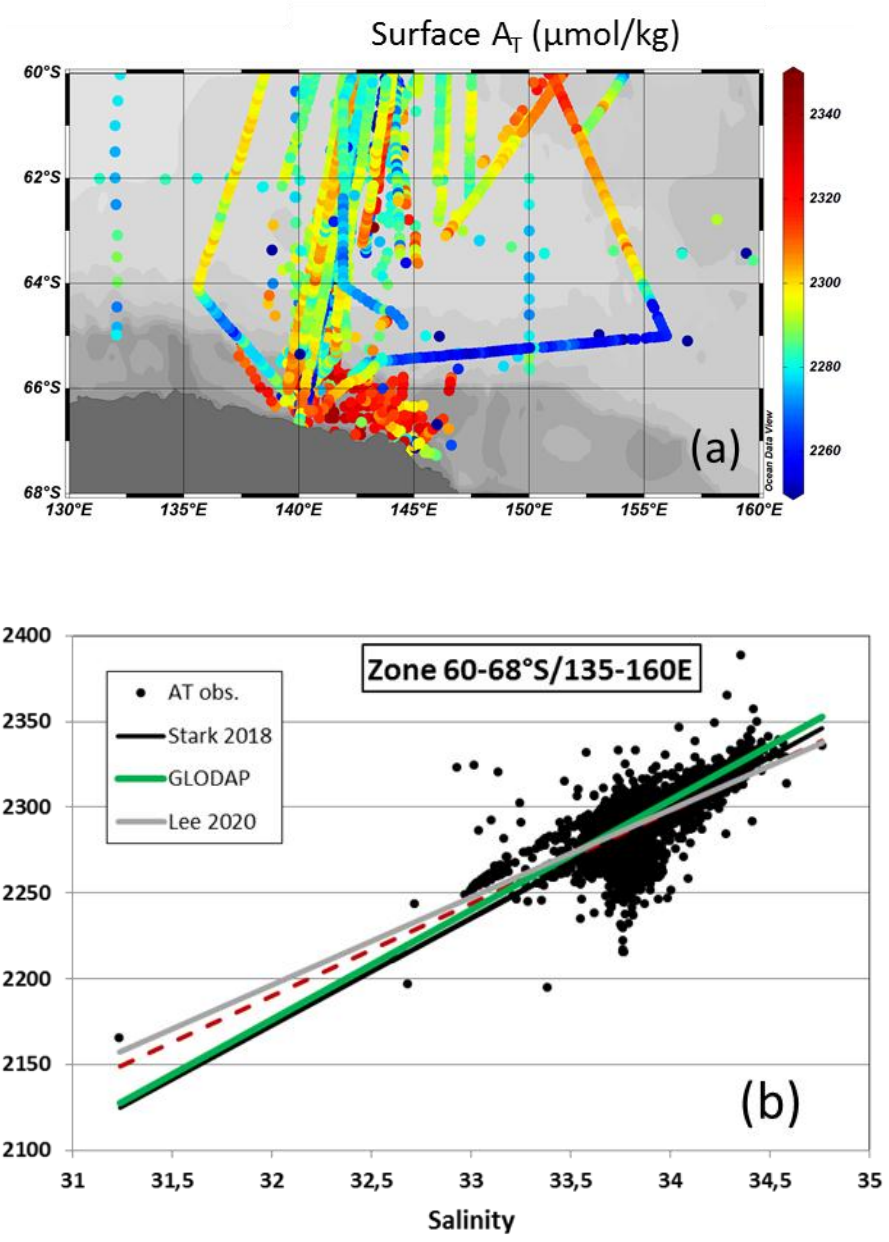


Figure S5: Maps of surface Chl-a concentration (mg m^{-3}) in January 2025, 2024 and 2002. Figures produced with ODV (Schlitzer, 2018) from data downloaded at https://resources.marine.copernicus.eu/ (OCEANCOLOUR_GLO_BGC_L4_MY_009_104), last access, 29-July-2025.

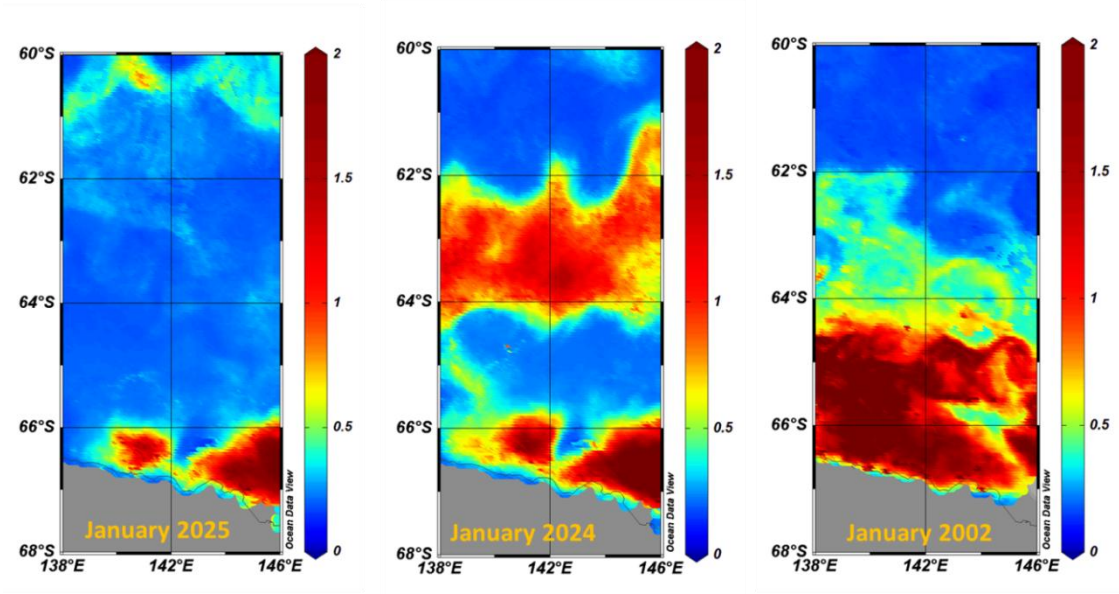


Figure S6: Time-series of (a) sea surface fCO_2 (µatm), (b) C_T (µmol kg^{-1}), (c) pH and (d) Ω_{ar} observed south of 64°S in 2024-2025 based on measured fCO_2 (grey circles) , BGC-Argo float pH data (open diamonds) and measured A_T C_T (orange triangle). Also shown are the results from the FFNN model (purple line).

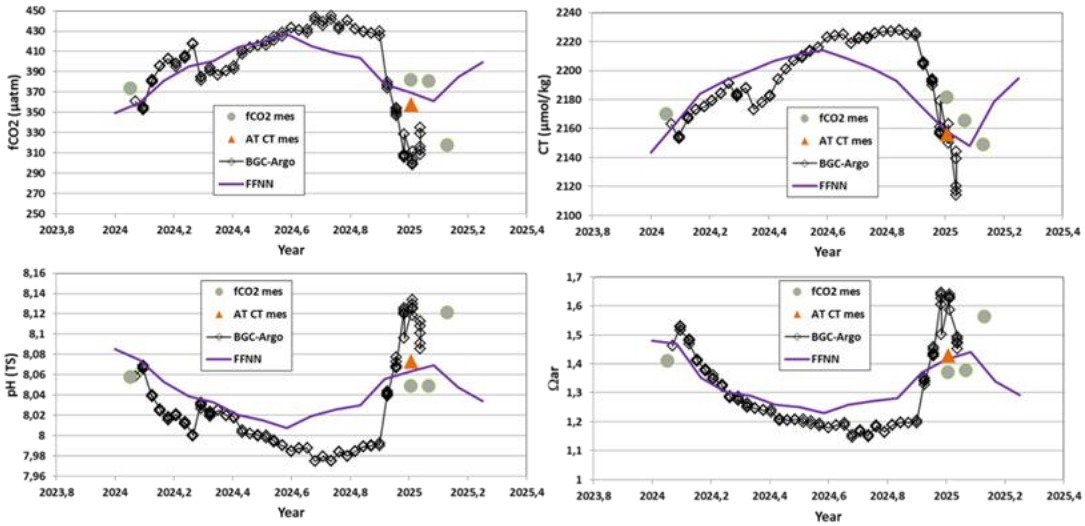


Figure S7: Same as figure 6 for the period 2000-2006 to highlight the anomaly in 2002. Time-series of (a) sea surface fCO_2 (µatm) and (b) C_T (µmol kg^{-1}) observed south of 65°S based on SOCAT fCO_2 data in summer (grey circles) and from A_T C_T data in summer (orange triangles) Also shown are the monthly values of the FFNN model (purple) and Chl-a concentrations (green, mg m^{-3}) at the same location. The red line in (a) is the atmospheric fCO_2.

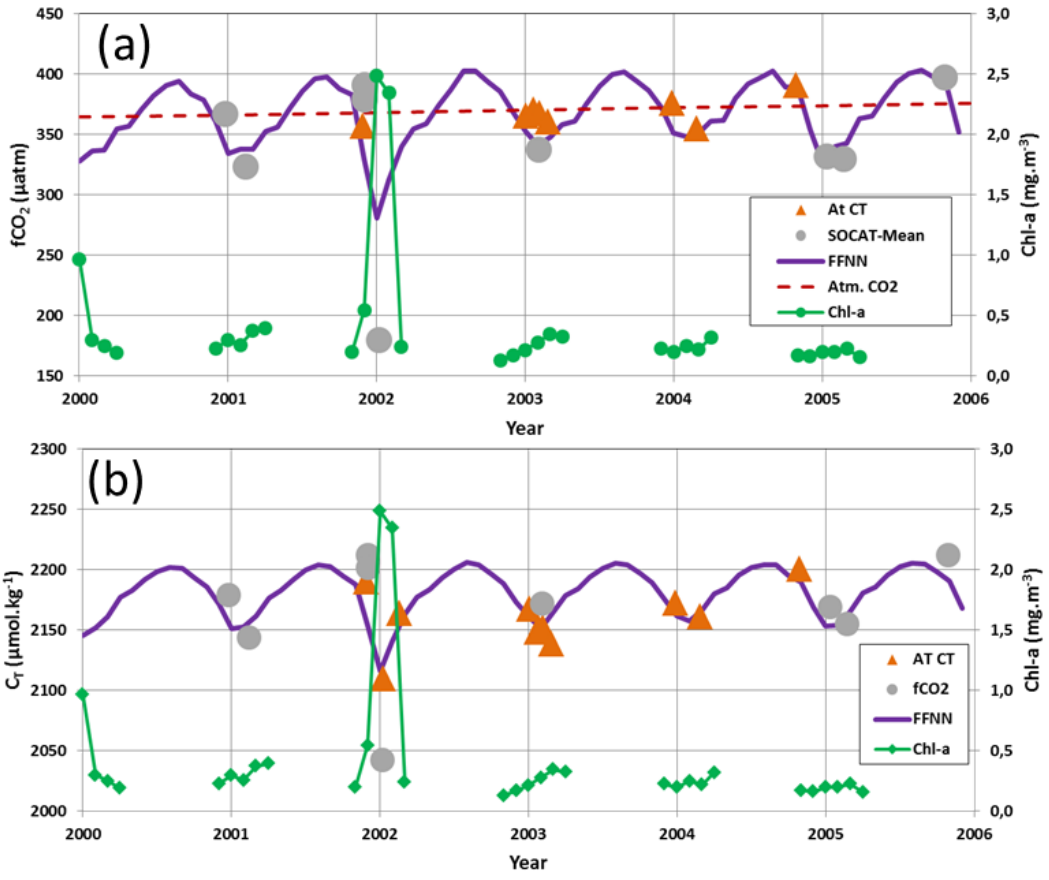


Figure S8: Time-series of air-sea CO_2 fluxes (mmolC m^{-2} d^{-1}) in January 1996-2025 from the FFNN model (centered at 65°S-140°E) and of the Chl-a concentrations (green, mg m^{-3}) at the same location. When Chl-a was high (e.g. 2002, 2015) the ocean was a stronger CO_2 sink.

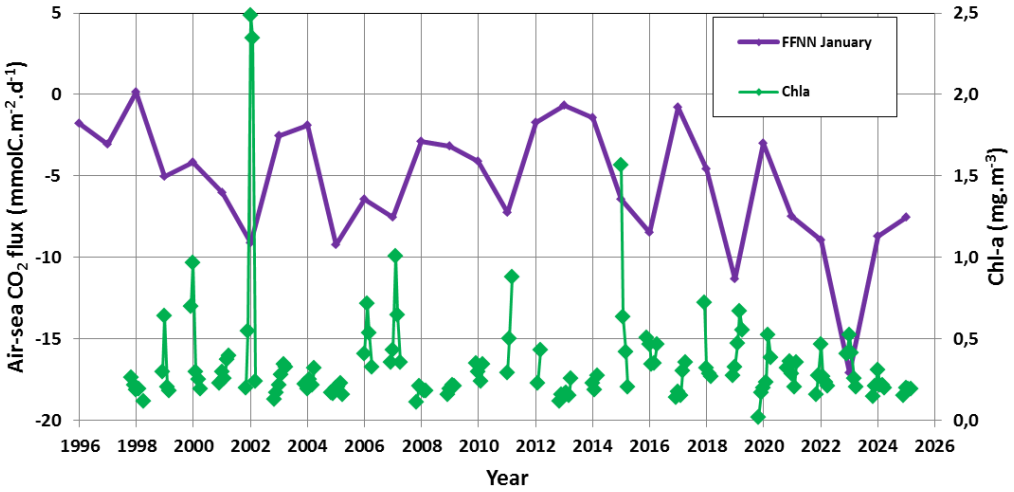


Figure S9: Maps of Ω_{ar} in January 2023 (left) and August 2023 (right) in the Adélie Land region based on the FFNN model. Note the different scales. During austral winter Ω_{ar} < 1.3. In summer Ω_{ar} presents high variability linked to biological processes. Figures produced with ODV (Schlitzer, 2018).

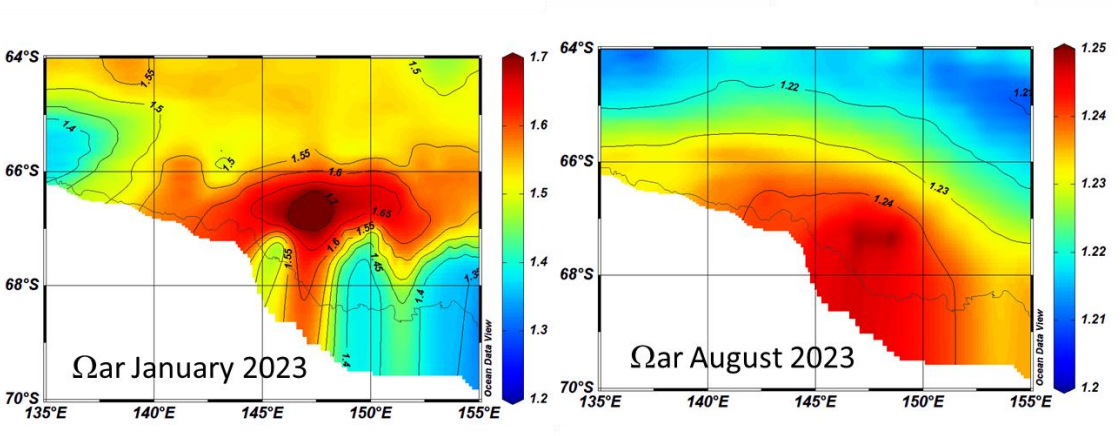


Figure S10: Time-series of (a) air-sea CO_2 fluxes (mmolC m^{-2} d^{-1}) and (b) Ω_{ar} in 1985-2025 from the FFNN model (centered at 65°S-140°E) in January (red) and August (blue). Dashed lines are the trends for each season (see Table 3). Here, we highlight the variability in austral summer.

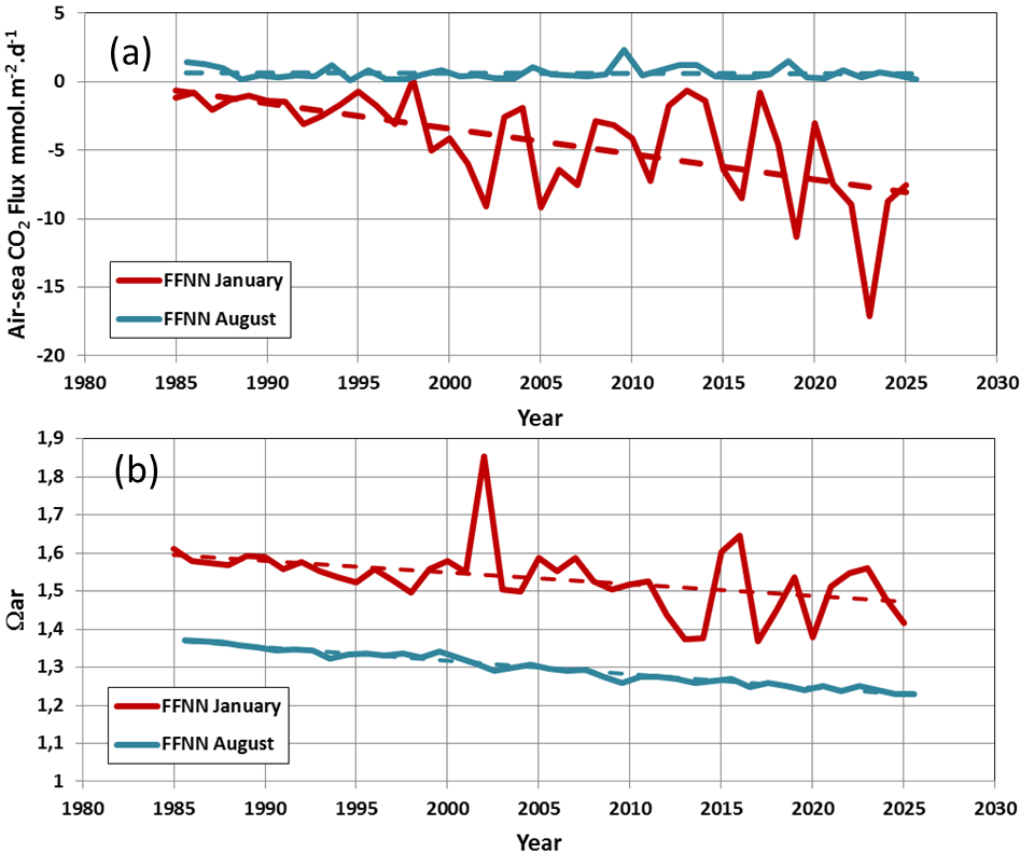


Figure S11: Time-series of the seasonal difference (August-January) for fCO_2 and C_T based on the FFNN model (centered at 65°S-140°E). The differences present high variability starting in 1998 when the model is constrained by Chl-a satellite data. No significant trends were observed but the seasonal amplitude was variable around 2000-2008 and 2015-2023.

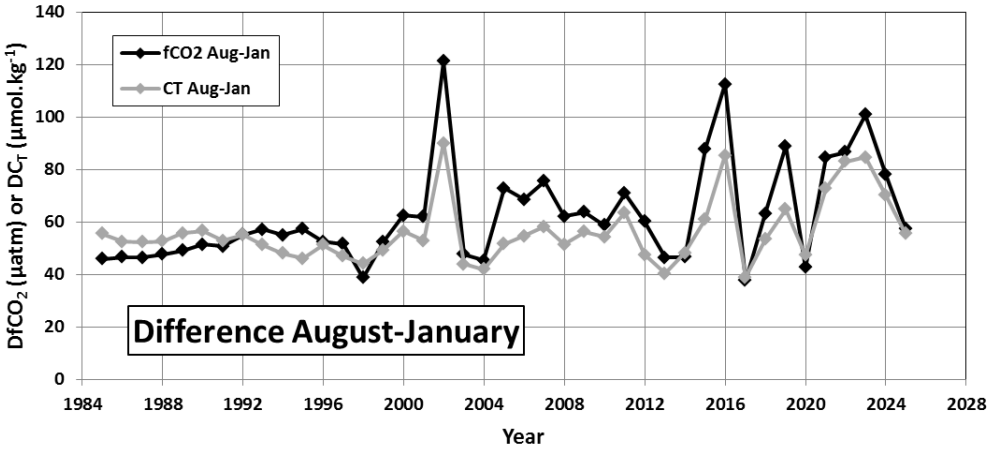


Figure S12: Time-series of Chl-a concentrations (mg m^{-3}) and C_{ant} (µmol kg^{-1}) derived from the BGC-Argo float (WMO 2903867) from January 2024 to February 2025. The C_{ant} concentrations are estimated below 100m and only for good pH_T data (Jan-2024/Jan-2025). Dots indicate the location of data. Figures produced with ODV (Schlitzer, 2018).

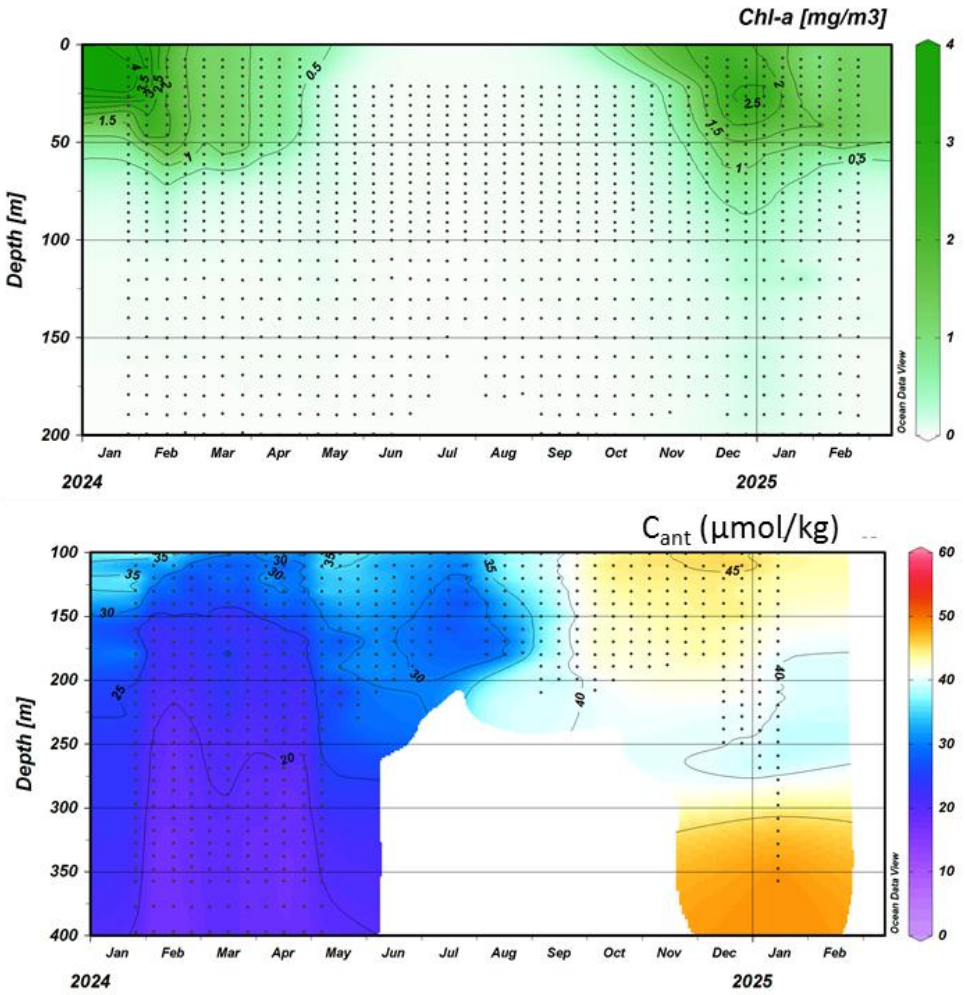


Figure S13: (a): Time-series of (a) Potential temperarure (°C), (b) salinity, (c) Oxygen (µmol kg^{-1}) and (d) C_T (µmol kg^{-1}) observed in 3 layers (below 100m) from 1994 to 2024. The trends are represented by dashed lines (see Table 4). In (d) are also shown the C_T concentrations in surface in August from the FFNN model (purple and dashed purple line is the C_T trend of 0.46 µmol kg^{-1} yr^{-1}). In 2013 an anomaly is identified for all properties in subsurface and sea surface C_T from the FFNN model is also slightly higher in 2013.

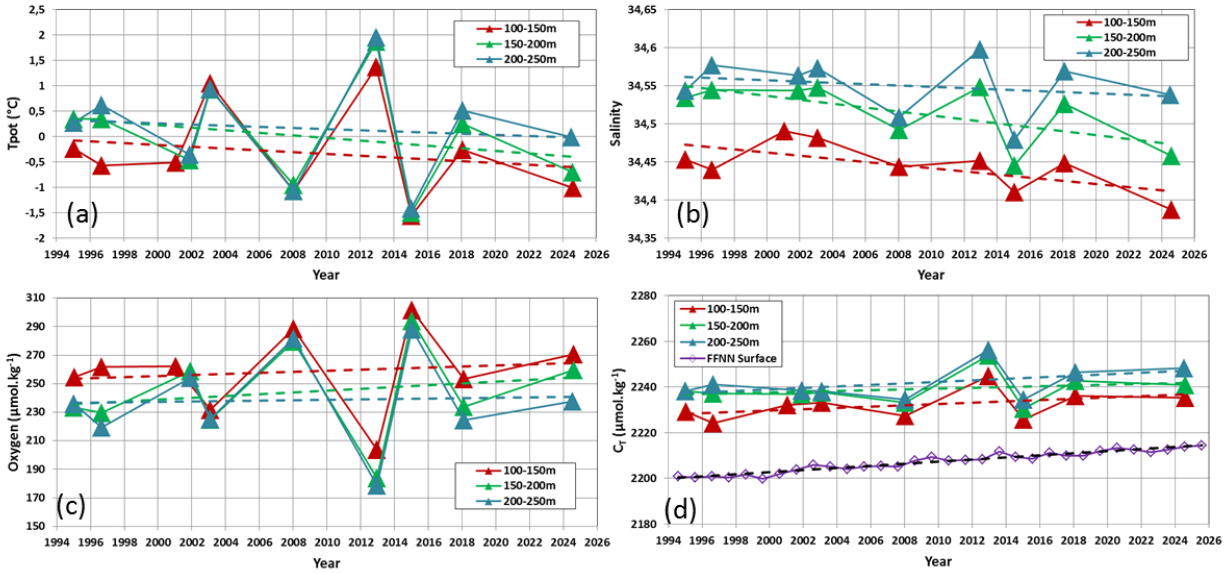


Figure S14: Sea surface δ13C (per mill) observed in August 1996, January 2003 and January 2025 south of 62°S in the Adélie Land region. The decrease of δ13C from 2003 to 2025 (same season) of -0.27 on average is linked to the anthropogenic CO_2 uptake (i.e. a Suess effect of -0.0123 yr^{-1}).

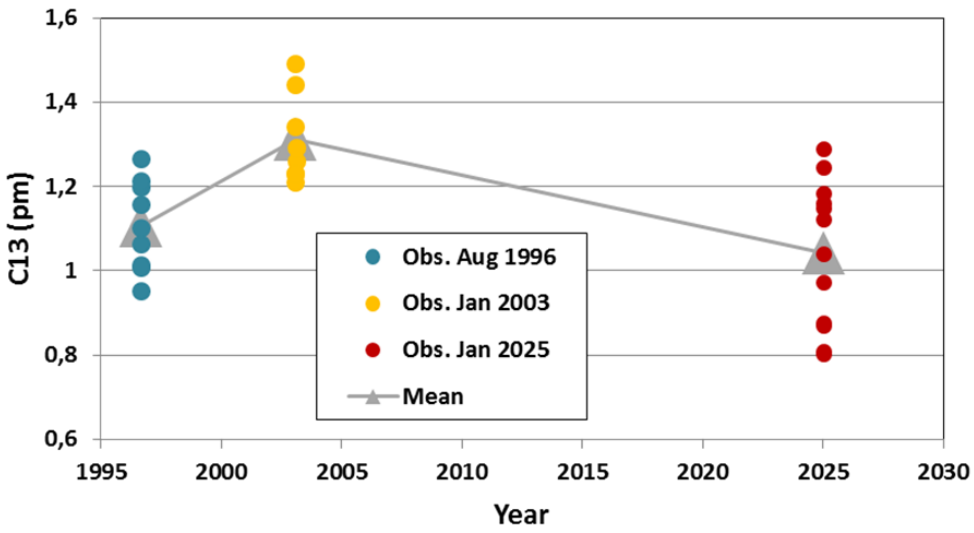


Figure S15: Time-series of C_T concentrations (µmol kg^{-1}) based on the FFNN model (purple) and the reconstruction for August using C_{ant} fitted (C_{ant} fit, red line, see Eq. 2,) and their difference (grey right axis). The dashed line is the FFNN trend (0.44 µmol kg^{-1} yr^{-1}).

